Journal of Pathology
J Pathol May 2021; **254:** 92–102
Published online 24 March 2021 in Wiley Online Library (wileyonlinelibrary.com) DOI: 10.1002/path.5640

ORIGINAL PAPER

Human cytomegalovirus infection is associated with increased expression of the lissencephaly gene *PAFAH1B1* encoding LIS1 in neural stem cells and congenitally infected brains

Maude Rolland[1†], Hélène Martin[1], Mathilde Bergamelli[1], Yann Sellier[2,3], Bettina Bessières[2,3], Jacqueline Aziza[4], Alexandra Benchoua[5], Marianne Leruez-Ville[2,3], Daniel Gonzalez-Dunia[1*] and Stéphane Chavanas[1*‡]

[1] *Centre for Pathophysiology Toulouse-Purpan (CPTP), INSERM, CNRS, University of Toulouse, Toulouse, France*
[2] *Hôpital Necker-Enfants Malades, Assistance Publique-Hôpitaux de Paris, Paris, France*
[3] *Université Paris Descartes, Paris, France*
[4] *Département d'Anatomie Pathologique, IUCT-Oncopôle Toulouse, Toulouse, France*
[5] *CECS, I-STEM, AFM, Corbeil-Essonnes, France*

**Correspondence to: S Chavanas, Toulouse NeuroImaging Centre (TONIC), UMR1214, INSERM, University of Toulouse, 31024, Toulouse, France. E-mail: stephane.chavanas@inserm.fr; or D Gonzalez-Dunia, Centre for Pathophysiology Toulouse-Purpan (CPTP), INSERM, CNRS, University of Toulouse, 31024, Toulouse, France. E-mail: daniel.dunia@inserm.fr*

†Current address: Laboratory of Molecular Immunology & Signal Transduction, GIGA Institute, University of Liège, 4000, Liège, Belgium
‡Current address: Toulouse NeuroImaging Centre (TONIC), UMR1214, INSERM, University of Toulouse, 31024, Toulouse, France.

Abstract

Congenital infection of the central nervous system by human cytomegalovirus (HCMV) is a leading cause of permanent sequelae, including mental retardation or neurodevelopmental abnormalities. The most severe complications include smooth brain or polymicrogyria, which are both indicative of abnormal migration of neural cells, although the underlying mechanisms remain to be determined. To gain better insight on the pathogenesis of such sequelae, we assessed the expression levels of a set of neurogenesis-related genes, using HCMV-infected human neural stem cells derived from embryonic stem cells (NSCs). Among the 84 genes tested, we found dramatically increased expression of the gene *PAFAH1B1*, encoding LIS1 (lissencephaly-1), in HCMV-infected versus uninfected NSCs. Consistent with these findings, western blotting and immunofluorescence analyses confirmed the increased levels of LIS1 in HCMV-infected NSCs at the protein level. We next assessed the migratory abilities of HCMV-infected NSCs and observed that infection strongly impaired the migration of NSCs, without detectable effect on their proliferation. Moreover, we observed increased immunostaining for LIS1 in brains of congenitally infected fetuses, but not in control samples, highlighting the clinical relevance of our findings. Of note, *PAFAH1B1* mutations (resulting in either haploinsufficiency or gain of function) are primary causes of hereditary neurodevelopmental diseases. Notably, mutations resulting in *PAFAH1B1* haploinsufficiency cause classic lissencephaly. Taken together, our findings suggest that *PAFAH1B1* is a critical target of HCMV infection. They also shine a new light on the pathophysiological basis of the neurological outcomes of congenital HCMV infection, by suggesting that defective neural cell migration might contribute to the pathogenesis of the neurodevelopmental sequelae of infection.

Keywords: cytomegalovirus; LIS1; *PAFAH1B1*; *DCX*; congenital infection; neuronal migration

Received 17 January 2020; Revised 2 February 2021; Accepted 5 February 2021

No conflicts of interest were declared.

Introduction

Human cytomegalovirus (HCMV) is a beta herpesvirus with a worldwide distribution and an estimated global seroprevalence of 83% in the general population [1]. Congenital HCMV infection of the central nervous system is a leading cause of permanent sequelae (0.1–0.2% of all live births) [2].

More specifically, 10% of congenitally infected newborns are symptomatic at birth [2]. Most of them (60–90%) and 10–15% of those with asymptomatic infection develop one or more long-term neurological sequelae, such as mental retardation, psychomotor retardation, sensorineural hearing or vision loss, or cerebral palsies [2,3].The most severely affected cases show brain development abnormalities such as lissencephaly or polymicrogyria [3]. A retrospective review reported that 10 out of 15 (66%) infants congenitally infected by HCMV showed polymicrogyria or abnormal gyral patterns [3,4]. Lissencephalic brains are characterised

by a smooth surface, whereas excessive abundance of gyri is found in polymicrogyria. These features are indicative of abnormal migration of neural cells (reviewed in refs 5 and 6), as observed in hereditary lissencephalies. Hereditary lissencephalies are monogenic disorders that show considerable clinical, genetic, and allelic heterogeneity, but which, however, are all characterised by defective neuronal migration during development [7]. Indeed, the sequential and finely synchronised migration of neural progenitors, radial glia cells, and neurons are all critical events for proper brain development [5,6].

Direct infection of neural progenitor cells by HCMV in the developing brain plausibly contributes to the neurological sequelae due to HCMV congenital infection [8–11]. In particular, HCMV infection of neural progenitors was found to perturb their self-renewal and polarisation [12], apoptosis [13], or differentiation [8,10,12–14]. To date, however, no evidence has been reported showing that HCMV infection indeed affects neural cell migration in the developing brain [15].

In this study, we assessed the abnormally expressed genes in HCMV-infected human neural stem cells derived from embryonic stem cells (NSCs) and found that infection causes abnormal expression of *PAFAH1B1*, the principal causative gene for hereditary lissencephalies.

Materials and methods

Ethics statement

Use of NSCs was approved by the French regulatory authorities (Agence de la Biomédecine, # SASB092 0178S). Collection of brain histological samples was coordinated by Necker Hospital, AP-HP (Assistance Publique – Hôpitaux de Paris, Agence de la Biomédecine, # PFS-15009). Written informed consent was obtained from all study participants prior to sample collection. All samples were anonymised.

Cells, viruses, and reagents

NSCs, human immortalised fibroblast MRC-5 cells, and human invasive proliferative extravillous cytotrophoblast (HIPEC) cells were grown *in vitro* as detailed elsewhere [11,16]. In brief, NSCs were seeded at 100 000 cells/cm^2 and maintained in growth medium consisting of DMEM/F12/Neurobasal medium (Life Technologies, Carlsbad, CA, USA) mixed at a ratio of 1/1/2 (v/v/v) in the presence of N2 and B27 supplements (Life Technologies), FGF2 (10 ng/ml), EGF (10 ng/ml), and BDNF (20 ng/ml), all from Peprotech, Rocky Hill, NJ, USA. Culture supports were first coated using 0.05% polyornithine (PO) (Sigma, St Louis, MO, USA), followed by mouse laminin (1 µg/cm^2) (Roche, Basel, Switzerland), both diluted in PBS. NSC cultures were checked for the absence of mycoplasma (Plasmotest; Invivogen, Toulouse, France). The MRC-5 line (CCL171; ATCC, Manassas, VA, USA) was cultured in DMEM containing 10% bovine calf serum (Life Technologies). The HIPEC line (a gift from T Fournier, INSERM UMR-S1139, Paris Descartes University, Paris, France) was cultured in DMEM/F12 (1/1), supplemented with 10% bovine calf serum.

We used the VHL/E HCMV strain (a gift from C Sinzger, Ulm, Germany) at low passage (<8) of amplification in MRC-5 cells and the AD169 HCMV strain (ATCC VR538). Preparation and titration of viral stocks and UV irradiation of viral inoculums were as detailed elsewhere [11]. Titration of viral suspensions was performed by immunofluorescence analysis on MRC-5 cells 24 h post-infection, using an antibody against HCMV immediate-early antigen (IE). We used primary antibodies specific to IE (mouse monoclonal; bioMérieux, Marcy l'Etoile, France), LIS1 (rabbit polyclonal, ab2607; Abcam, Cambridge, UK), DCX (rabbit polyclonal, ab18723; Abcam), Ki-67 (rabbit monoclonal; Merck Life Science, Dorset, UK), and alpha-tubulin (rabbit monoclonal, 11H10; Cell Signaling Technology, Leiden, The Netherlands). Secondary antibodies were conjugated either with horseradish peroxidase (Promega, Madison, WI, USA) for western-blot assays and immunohistochemistry (IHC) or with Alexa-488, -555 or -633 fluorophores (Life Technologies) for immunofluorescence analyses.

mRNA analysis

NSCs were infected at a multiplicity of infection (MOI) of 10 using the AD169 or VHL/E strains or left uninfected and harvested 72 h post-infection (pi). Total RNA was extracted from actively growing NSCs (i.e. at approximately 75% confluency) using Trizol (Life Technologies) according to the supplier's recommendations. Ten micrograms of RNA was reverse-transcribed in the presence of oligo-dT using Superscript III reverse transcriptase (Life Technologies). A first screen was performed using the RT^2 Profiler Neurogenesis kit (Qiagen, Hilden, Germany) according to the supplier's recommendations. Next, quantitative real-time PCR (qPCR) assays were performed as devised elsewhere [11] using Takyon qPCR mastermix (Eurogentec, Liège, Belgium), oligonucleotide probes (Qiagen) specific to *PAFAH1B1* and *RPLP0* (ribosomal protein, large, P0), as a reference gene, and an LC480 system (Roche). For each experiment, two batches of NSCs were infected separately. For each, RT-qPCR was duplicated. Culture passage was between 10 and 12.

Western blotting

NSCs were infected at an MOI of 10, or left uninfected, and harvested 72 h pi. Cell extract preparations and western blotting analyses were performed as detailed elsewhere [11]. Detection was carried out using a chemiluminescence kit (Sigma). Analyses were performed with a Chemidoc system (Bio-Rad, Hercules, CA, USA). Densitometry analyses were performed using ImageJ software [17].

Immunofluorescence

Cells were cultured on coverslips, fixed in 4% formaldehyde for 20 min at 4 °C, and permeabilised in 0.3% Triton X-100 for 15 min at room temperature. Blocking buffer was PBS containing 5% FCS. Primary antibodies diluted in blocking buffer were applied overnight at 4 °C. Antibodies to IE, LIS1, DCX, Ki-67, and alpha-tubulin were diluted 500-, 250-, 250-, 100-, and 50-fold, respectively. Secondary antibodies diluted in blocking buffer were applied for 1 h at room temperature. After three washes with blocking buffer and three washes with PBS, cells were counterstained with 1 μg/ml DAPI (Sigma) and washed again three times with PBS before mounting the coverslips onto glass slides. Examination was performed using an LSM 710 confocal microscope (Zeiss, Oberkochen, Germany). Image processing was performed using either ImageJ (maximal-intensity projections, measurements of length) or Imaris (Oxford Instruments, Abingdon, UK) (3D reconstructions). The relative number of Ki-67-positive cells was assessed by manual counting from captures of five visual fields, each containing 100–200 cells.

Cell migration assays

Cell migration assays were performed using the Oris Cell Migration Assay (Platypus Technologies, Madison, WI, USA) according to the supplier's recommendations. NSCs were plated in dedicated 96-well plates at a density of 50 000 cells per well, in the presence of silicone stoppers at the centre of each well, to generate a cell-free exclusion zone. The next day, NSCs were infected by HCMV; then the culture medium was replaced with fresh medium containing laminin (1 μg/cm^2) and the stoppers were removed, allowing for NSCs to colonise the exclusion zone. Brightfield pictures of each well were taken each day thereafter over 4 days, using an Apotome Axio-observer microscope (Zeiss). The area of the remaining cell-free zone was measured using ImageJ software. The growth rate of control or HCMV-infected NSC cultures was also assessed in parallel experiments through DAPI staining and counting of the nuclei over time, by using an automated ArrayScan microscopy device (Cellomics, Thermo Fisher Scientific, Waltham, MA, USA).

PAFAH1B1 silencing

NSCs were seeded at a density of 60 000 per cm^2 in 24-well plates. HIPEC cells were seeded at a density of 25 000 per cm^2 in 24-well plates. The day after, fresh medium containing 100 pmol of non-targeting- or LIS1-siRNAs was added to each well according to the supplier's recommendations (Horizon Discovery, Cambridge, UK) and 24 h later, cells were infected at an MOI of 10 or left uninfected. Immunofluorescence analysis was next performed at 4, 24, and 72 h pi. To assess cell death, cells were incubated for 30 min at 37 °C in growth medium supplemented with the Image-iT™ DEAD reagent (Life Technologies) at a final concentration of 100 nM, before carrying out immunofluorescence assays as detailed above.

Immunohistochemical analyses

Brain tissue biopsies were collected from four human fetuses electively aborted because of HCMV infection and from two controls aborted for Di George syndrome with associated cardiopathy (control case 1200496) or for premature rupture of membranes, anamnios, and chorioamnionitis (control case 1200094). Immunohistochemical brain analysis of controls and HCMV cases was performed on sections cut at 8 μm from paraffin blocks, using standard methods. Antigen was retrieved through two consecutive incubations (11 and 10 min) in a microwave oven for DCX or one 40-min incubation at 95 °C in a heating bath for LIS1. Endogenous peroxidase activity and biotin were blocked by using the avidin–biotin and peroxidase blocking reagents (Vector Labs, Burlingame, CA, USA) for 10 min at room temperature. Primary antibodies were diluted 800-fold (DCX) or 250-fold (LIS1) in blocking buffer (3% BSA in PBS). Antibody specificity was ascertained by parallel staining experiments using either no primary antibody or a non-specific isotype control.

Staining for LIS1, DCX, and Mayer's haematoxylin counterstain was performed using an Autostainer device (Dako, Glostrup, Denmark), and resulting slides were scanned using a Panoramic 250 system (3D Histech, Budapest, Hungary) and analysed with the dedicated software (3D Histech).

Statistical analysis

Statistical analyses were performed using the StatEL plugin (Adscience SARL, Paris, France) for Excel (Microsoft, Redmond, WA, USA), using the Kruskal–Wallis test. Unless otherwise specified, error bars show 5% confidence intervals (CIs).

Results

In the search for genes with altered expression in HCMV-infected NSCs, we performed mRNA analysis using a dedicated array allowing us to analyse a set of 84 genes related to neurogenesis. We used an MOI of 10 with respect to titration in MRC-5 cells, a condition that led to approximately 30–40% of NSCs displaying positive IE immunostaining 72 h post-infection. We reported previously that infection at this MOI does not result in any increased apoptosis [11]. Most of the genes of this array showed only minor changes in transcript levels upon HCMV infection (supplementary material, Table S1). Yet we found that the steady-state levels of mRNA of the genes *ACHE*, *APOE*, *S100A6*, and *PAFAH1B1* were increased by 3.68-, 4.65-, 5.73-, and 56.67-fold, respectively, in infected NSCs compared with uninfected control cells (Figure 1A). We focused

on *PAFAH1B1* because this gene is the principal causative gene of lissencephalies (as reviewed in refs 7 and 18) and because lissencephalic brain is frequently reported in severe congenital HCMV infection. Therefore, we next carried out RT-qPCR to validate the result of the first screen, using mRNA extracted from NSCs infected by two different HCMV strains, AD169 and VHL/E. Consistent with the array results, we found that the steady-state levels of *PAFAH1B1* mRNA were increased 37.67- and 41.32-fold in NSCs infected by AD169 or VHL/E, respectively, compared with the uninfected controls (Figure 1A). Notably, no significant change in the *PAFAH1B1* mRNA levels was detected in NSCs treated by UV-irradiated viral particles of the two strains.

This prompted us to investigate the levels of the protein encoded by *PAFAH1B1*, namely LIS1, in NSCs. In uninfected NSCs, western blotting revealed the expression of only minute amounts of LIS1 (45 kDa) (Figure 1B) and no detectable LIS1 was observed by immunofluorescence analysis (Figure 1C, top row). In contrast, both western blotting and immunofluorescence revealed a dramatic increase of LIS1 protein levels in HCMV-infected NSCs, compared with uninfected control cells or with NSCs exposed to a UV-irradiated viral inoculum (Figure 1B,C). Interestingly, immunostaining for HCMV immediate-early antigen (IE) revealed that increased staining for LIS1 was only observed in infected NSCs and not in their neighbouring uninfected counterparts (Figure 1C,D). Further examination of infected cells at higher magnification or with 3D reconstructions revealed dot-like cytoplasmic LIS1 immunostaining, distributed as linearly arranged foci, indicative of cytoskeletal association (Figure 1D and supplementary material, Movies S1–S4). In most infected cells, a greater density of fluorescence spots was observed in the perinuclear zone.

LIS1 is an atypical microtubule-associated protein [19,20]. To gain insight into the impact of HCMV infection on the microtubule network of NSCs, we carried out immunofluorescence analysis of tubulin in infected NSCs. We detected no difference in the shape of the microtubule network in infected NSCs compared with the controls (supplementary material, Figure S1). This suggested that microtubules were not impacted by infection at a detectable level in cultured NSCs and that the pattern of LIS1 staining in infected NSCs is not the consequence of a disrupted microtubule network.

We next investigated the consequence of infection by HCMV on *PAFAH1B1* expression in human fetal lung MRC-5 fibroblasts. mRNA RT^2 profiling (supplementary material, Table S2) and immunofluorescence analysis (supplementary material, Figure S2) showed that *PAFAH1B1* mRNA levels and LIS1 immunostaining were increased 8.5-fold in infected MRC-5 cells compared with uninfected MRC-5. Hence, increased LIS1 expression upon HCMV infection did not seem to be specific to NSCs.

Because poly(micro)gyria and lissencephaly are considered as neural cell migration disorders [5,6,21], we investigated possible changes in the migratory capacities of NSCs upon infection by HCMV. Towards this aim, we used the Oris cell migration assay, allowing reliable assessment of the ability of infected or control NSCs to fill an exclusion zone created by a silicone stopper present in the centre of the well during seeding and removed after infection. We observed that infected NSC cultures were unable to efficiently colonise the exclusion zone after 4 days, a stage when their uninfected counterparts had almost filled the whole area (Figure 2A,B). This migration deficit of infected cells was not due to cell lysis, since 4 days is an insufficient timescale for the completion of a full HCMV lytic cycle in NSCs, as shown previously [11]. To ensure that this effect was not the consequence of defective cell proliferation upon infection, we assessed the growth rates of infected and control NSCs over time and found no significant differences (Figure 2C). It has been shown that HCMV infection can have variable outcomes on the cell cycle, by either blocking or supporting proliferation [15,22,23]. Therefore, we carried out immunofluorescence analysis of the Ki-67 proliferation marker using HCMV-infected NSCs. We found no significant difference in the abundancy of Ki-67^+ cells between uninfected cultures, cultures infected by the strain AD169 or by the strain VHL/E, or cultures treated with irradiated VHL/E viral particles (supplementary material, Figure S3). Importantly, we detected many double-positive IE^+, Ki-67^+ cells among NSCs infected by the VHL/E or the AD169 strain, indicating that infected NSCs were still able to undergo the cell cycle. Therefore, the results of the migration assays most likely revealed impaired mobility of HCMV-infected NSCs. NSCs treated with a UV-irradiated viral inoculum showed no differences with the controls, indicating that only replication-competent HCMV was able to disrupt NSC mobility. Taken together, these findings show that HCMV infection impairs the migration of NSCs *in vitro*. Next, we investigated whether counteracting LIS1 overexpression would restore the migratory capacity of HCMV-infected NSCs. To this aim, we treated NSC cultures with either siRNAs specific to LIS1 or non-targeting control siRNAs. The two siRNAs shared identical chemistry and formulation. According to the supplier, a 72-h delay is required to achieve a good efficacy of silencing; therefore we started with siRNA treatment and then inoculated the cultures with HCMV. We observed a drastically different outcome for the survival of infected NSCs upon treatment with either LIS1- or control siRNAs. Indeed, we observed dramatic levels of cell death in HCMV-infected NSCs when they were exposed to the LIS1 siRNA, as evidenced by the positive staining with the Image-iT™ DEAD reagent, which only enters into dying cells (supplementary material, Figure S5). Cell death was so massive that it could be only evidenced at 4 h pi and cells were completely lost thereafter. In contrast, treatment with the non-targeting siRNA did not result in a detectable effect on cell survival. Interestingly, there was no impact on the survival of uninfected NSCs upon exposure to either LIS1- or

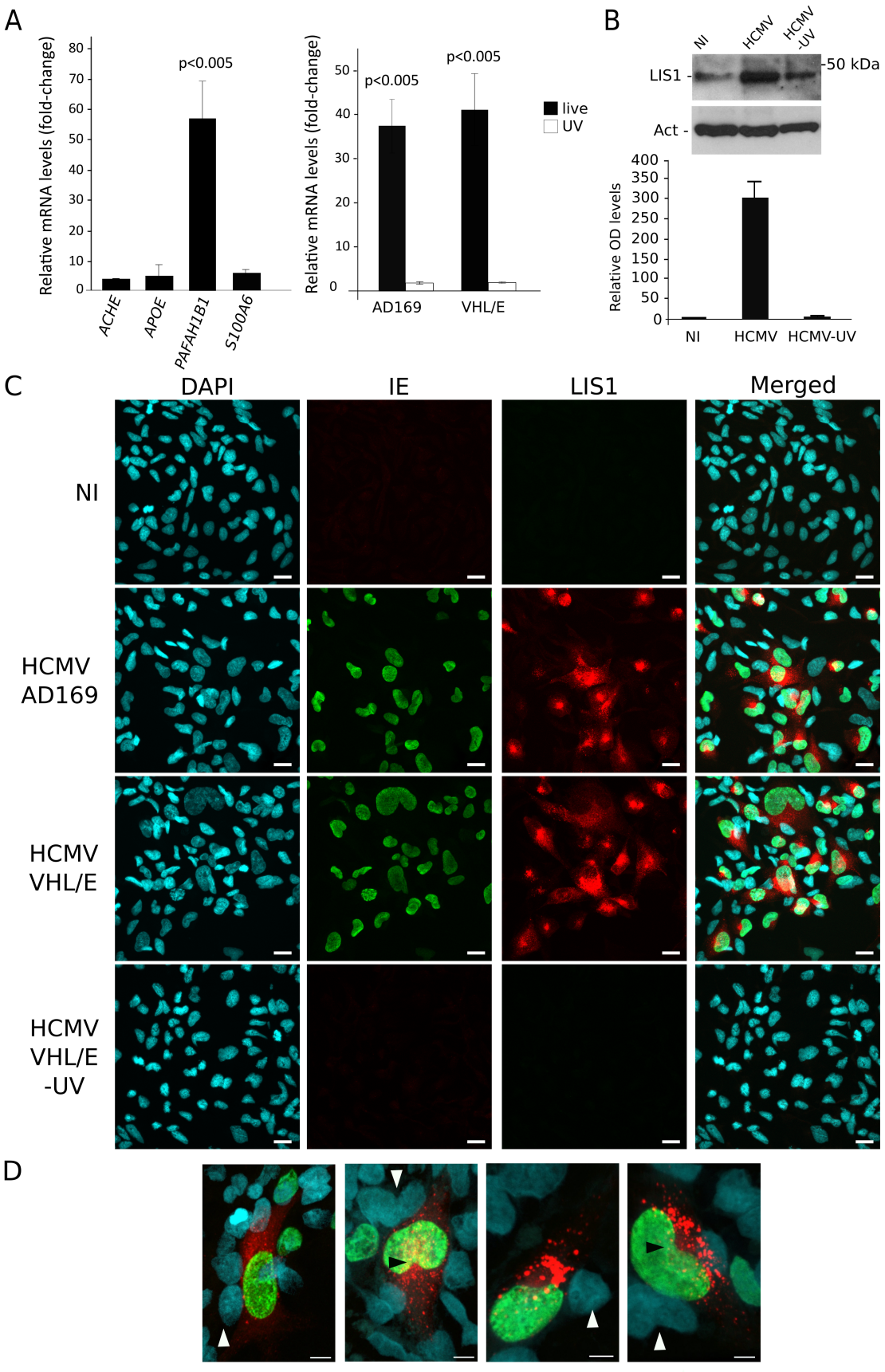

Figure 1 Legend on next page.

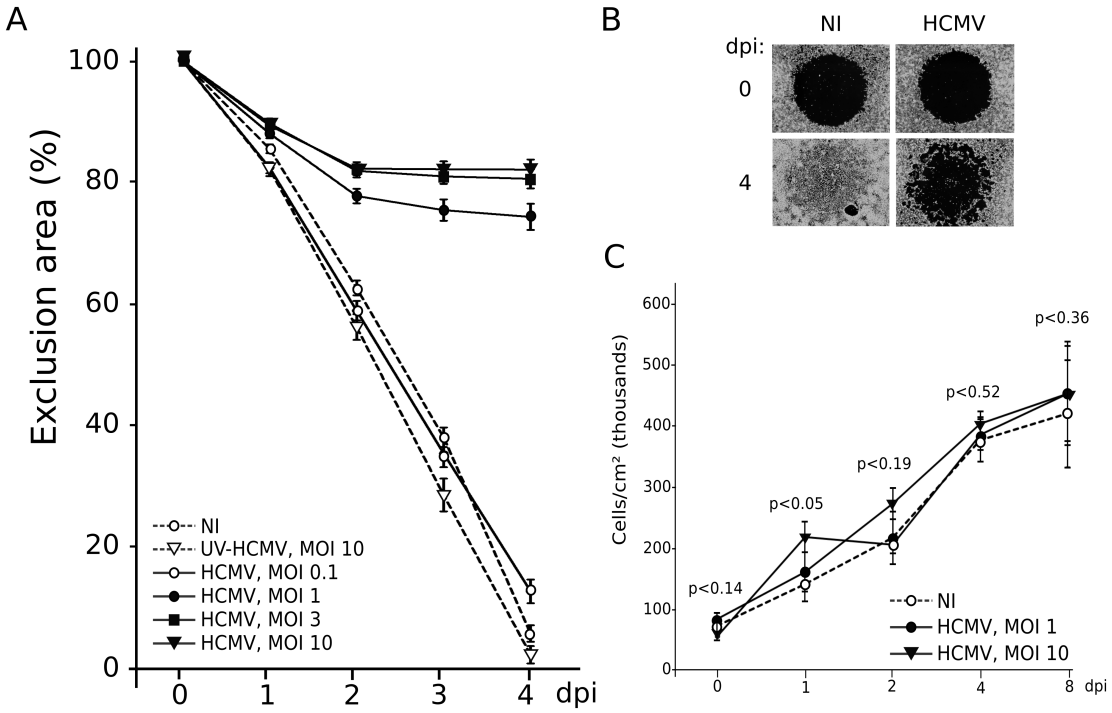

Figure 2. Defective migration ability of HCMV-infected NSCs. (A) Representative cell migration assay (Oris) showing defective migration on a laminin substrate of NSCs infected at effective MOI (1, 3, 10) compared with uninfected NSCs (NI) or NSCs exposed to UV-irradiated HCMV (HCMV-UV), or infected with ineffective MOI (0.1). The remaining cell-free area, which is expressed as a percentage of that before infection (day 0), is shown. At least six identical replicate wells were seeded for each experimental condition and three separate experiments were performed with similar results. (B) Representative views of the exclusion zone in the presence of NSCs labelled by calcein (1 h at 37 °C), uninfected (NI) or infected (HCMV), at an MOI of 10, at days 0 and 4 pi. (C) Analysis of the growth rates of HCMV-infected or uninfected control NSC cultures. The number of cells per cm^2, as assessed by counting of nuclei after DAPI staining, is shown. NSCs were cultured in triplicate 0.35 cm^2 wells and the experiment was performed twice.

non-targeting siRNAs. To follow up this observation and assess its specificity, we investigated the outcomes of LIS1 siRNA treatment using another HCMV-permissive cell line of non-neuronal origin, namely the cytotrophoblast cell line HIPEC. Interestingly, HIPEC cells do not show detectable expression of LIS1, should they be infected or not. In this case, we did not observe any effect of LIS1 siRNA on the survival of HCMV-infected HIPEC cells (supplementary material, Figure S5). This result ruled out the possibility of a direct cytotoxic effect of the LIS1 siRNA solution. Taken together, our results suggest that LIS1 overexpression is critical for the survival of HCMV-infected NSCs.

To assess the clinical relevance of our findings concerning LIS1 upregulation upon infection, we next explored LIS1 levels in histological sections of brain from congenitally HCMV-infected fetuses ($n = 4$) compared with control samples ($n = 2$) with a matching

Figure 1. Enhanced *PAFAH1B1*/LIS1 expression in HCMV-infected human neural stem cells. (A) RT-qPCR analysis showing dramatically increased levels of *PAFAH1B1* transcripts in HCMV-infected NSCs (MOI 10) at 72 h post-infection (pi). Left: RT^2 profiler analysis. The fold-change values of relative mRNA levels for each gene, compared with that from uninfected NSCs, are shown. Means ± CI of three independent experiments, two replicates per condition. Right: RT-qPCR analysis of *PAFAH1B1* mRNA levels in NSCs infected by HCMV strains AD169 (AD169) or VHL/E (VHL/E) (live, black boxes), or with UV-irradiated AD169 or VHL/E (UV, white boxes). Fold-change values of *PAFAH1B1* mRNA levels, compared with that from uninfected NSCs. Means ± CI of two independent experiments, two replicates per condition. (B) Representative western blot (top) and densitometry analysis (bottom) of three independent western blotting analyses of LIS1 levels in HCMV-infected (AD169 strain, MOI 10) NSCs (HCMV) compared with uninfected controls (NI) or with NSCs exposed to UV-irradiated HCMV (HCMV-UV) at 72 h pi. Error bars show SD. For densitometry analysis, data were normalised to actin levels and are expressed as relative densitometry units (DU), compared with uninfected cells arbitrarily set to 1. (C) Immunofluorescence analysis using antibodies specific to LIS1 (red) or IE (green) showing strong LIS1 immunostaining in NSCs infected by HCMV strain AD169 (AD169) or VHL/E (VHL/E) at an MOI of 10 (HCMV) compared with uninfected NSC cultures (NI) or with NSCs exposed to UV-irradiated VHL/E HCMV (HCMV-UV) at 72 h pi. This immunofluorescence analysis is representative of at least ten independent experiments, which gave identical results. Scale bar = 20 μm. Cyan = DAPI counterstain. (D) Representative enlarged images of immunofluorescence analysis using antibodies specific to LIS1 (red) or IE (green). Images are maximal-intensity projections of *x/y* optical section stacks acquired by confocal microscopy, for four different infected cells. Note the cytoplasmic dot-like pattern of LIS1 immunostaining in HCMV-infected cells compared with non-infected cells (white arrowheads). The nucleus groove as seen in the second and fourth cells shown (black arrowheads) is typical of a productively infected cell. Scale bar = 10 μm. Cyan = DAPI counterstain.

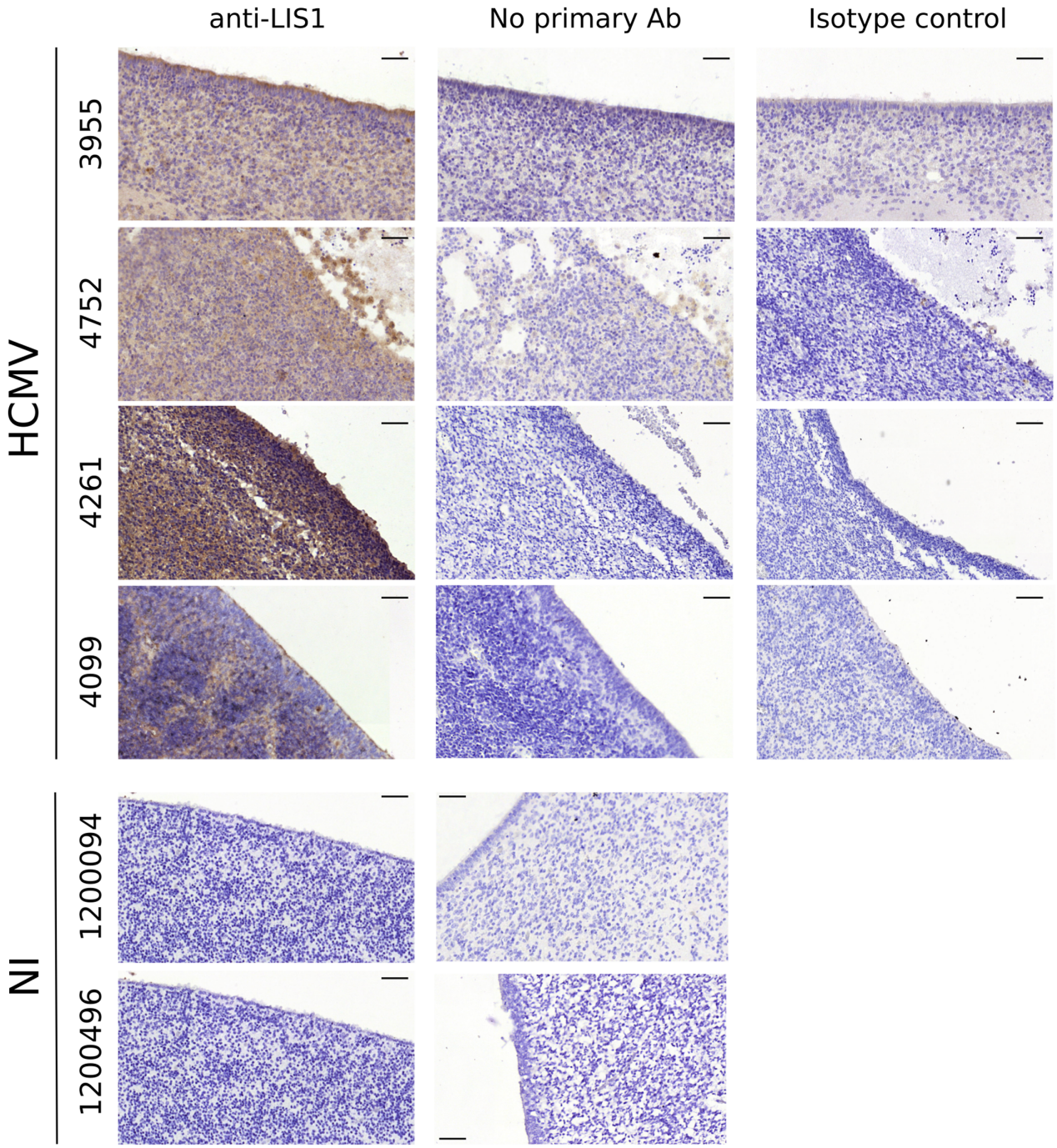

Figure 3. Increased levels of LIS1 in histological sections from HCMV-infected fetal brains. Representative results of immunohistochemical staining of brain sections from HCMV-infected fetuses (HCMV) or from controls (NI) using anti-LIS1 or no primary antibody or an isotype control. The reference number of each sample is indicated on the left of each row. The subventricular zone (SVZ) and the ependyma monolayer which segregates the SVZ from the ventricular space are shown. Note that cells strongly immunoreactive to anti-LIS1 antibody are detected in the periventricular areas and in ependyma in infected cases but not in controls. Scale bar = 50 μm.

gestational age (23 weeks). All four infected cases presented (poly)microgyria, which was associated in three cases with lissencephaly (cases 4752, 4261, 4099), hallmarks of migration abnormalities [5]. They were associated with microcephaly (cases 4752, 3955), ventriculomegaly (cases 4752, 4261, 3955), vascular lesions (cases 4752, 4099, 3955), and/or intraventricular (case 4261) or subventricular (case 4099) haemorrhage. Detailed clinical features of these cases have been reported elsewhere [11]. There was no familial history of neurological abnormalities in any of the cases. Fetal infection by HCMV was evidenced by immunohistopathological analyses of the presence of IE^+ cells, as shown previously [11]. No genetic screen was performed, the aetiology of the disease being infection by HCMV.

LIS1 was barely detectable in controls, whereas sections from infected cases showed strongly increased

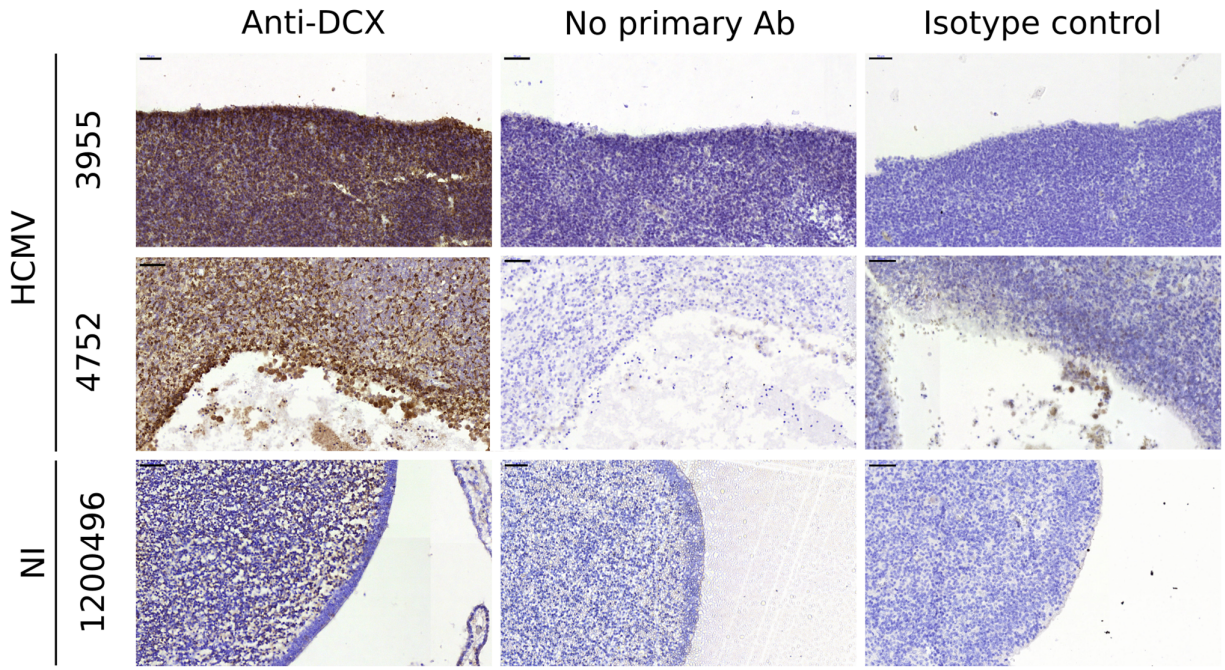

Figure 4. Increased levels of DCX in histological sections from HCMV-infected fetal brains. Representative results of immunohistochemical staining of brain sections from HCMV-infected fetuses (HCMV) or from controls (NI) using anti-DCX or no primary antibody or an isotype control. The reference number of each sample is indicated on the left of each row. Note that cells strongly immunoreactive to anti-DCX antibody are detected in the periventricular areas and in ependyma in infected cases but not in controls. Scale bar = 50 μm.

LIS1 levels throughout the parenchyma, particularly in the subventricular zone (SVZ) and the ependyma monolayer, which segregates the SVZ from the ventricular space (Figure 3). Notably, the SVZ is known to host the neural progenitors/stem cells [24].The validity of our histological staining was further ensured by staining of adjacent sections with an isotype control or by omission of the primary antibody, which were all, as expected, negative. These findings suggested that LIS1 was upregulated in all cells, infected or not, *in utero*. Our observation indicates that *PAFAH1B1* expression is abnormally increased in the brains of congenitally infected fetuses, thereby strongly supporting its association with the pathogenesis of the sequelae of the infection.

LIS1 is co-expressed and interacts physically with doublecortin (DCX), another microtubule-associated protein [25]. Similarly to *PAFAH1B1*, the gene *DCX* has been described as a causative gene for certain forms of lissencephalies (23%) [26]. In our initial screening, *DCX* mRNA levels tended to be increased in HCMV-infected versus uninfected NSCs (supplementary material, Table S1). Therefore, we investigated DCX levels, both in HCMV-infected NSCs and in the histological sections from infected cases or controls. We observed increased levels of DCX in HCMV-infected NSCs compared with the uninfected controls (supplementary material, Figure S4). It is noteworthy that DCX staining was punctate and mostly perinuclear, recalling that of LIS1. Not all infected NSCs, however, were positive for DCX. Immunohistochemical analysis was only possible for cases 3955 and 4752 because of the lack of available histological material for the other samples. We found strongly increased immunostaining for DCX throughout the brains of congenitally infected cases, whereas DCX expression was hardly detectable in control sections at this gestational age (Figure 4). These results suggest widespread overexpression of LIS1 and DCX in the parenchyma. It is noteworthy that no DCX expression was detectable for MRC-5 cells, whether infected or not, by mRNA (supplementary material, Table S2) or immunofluorescence analyses (not shown).

Discussion

In this study, we report that congenital HCMV infection is associated with strongly increased expression of *PAFAH1B1*/LIS1, both in human NSCs (Figure 1) and in congenitally infected fetal brains, as early as the 23rd week of gestation (Figure 3) [27].

We observed dramatically increased LIS1 levels in HCMV-infected NSCs. We previously reported that infection by HCMV triggered the activity of the nuclear receptor PPARγ in NSCs [11]. In contrast to that study, we did not detect any paracrine effect leading to increased LIS1 levels in the neighbouring uninfected NSCs. The pattern of LIS1 immunostaining in HCMV-infected NSCs is suggestive of an association with the cytoskeleton (Figure 1C,D). This finding is in agreement with previous studies showing a physical association of LIS1 with microtubules [28,29]. Moreover, we found that LIS1 concentrated as puncta, with a size reaching

up to 1.5 μm in diameter (Figure 1C), consistent with previous observations in COS-7 cells overexpressing LIS1 [28]. Perinuclear LIS1 immunolabelling observed in infected NSCs also agrees with previous work showing an association of LIS1 with the Golgi complex [30].

The molecular role of LIS1 has been extensively studied [19,20]. LIS1 is an adaptor for the microtubule motor dynein, which it maintains connected to microtubules, presumably acting as a 'propeller wheel' [27]. LIS1 is critical for cytoskeleton dynamics, nucleokinesis, and neural cell mobility [21]. Moreover, LIS1 is a downstream effector of reelin, a pivotal regulator of neuronal migration [31], and of platelet-activating factor (PAF), a lipid mediator regulating neuronal migration and neurite outgrowth [32,33]. LIS1 has been shown to reduce the rate of transition from growth to shortening of microtubules [29], a dynamic process that could not be detected in our immunofluorescence assay. Together, these studies point to LIS1 as a key effector of neural cell motility. We observed defective migration of HCMV-infected NSCs in a two-dimension assay, a model that does not take into account the possible contribution of glial cells in neural progenitor migration during neurodevelopment [34,35]. With our study, it is important to stress that current evidence does not allow us to establish any formal link between overexpressed LIS1 and altered migration of HCMV-infected NSCs. Using a lentiviral transduction strategy, we failed to generate viable NSCs ectopically expressing LIS1 at a level sufficient to cause a change in migration abilities. On the other hand, treatment with siRNA targeting LIS1 led to the specific death of infected NSCs. Therefore, it is not possible to formally conclude that LIS1 plays a role *per se* in defective migration of infected NSCs. Depending on the cell context, HCMV infection has been shown to exert opposite outcomes on cell migration. For instance, HCMV promotes the motility of monocytes through STAT1 activation [36] and also enhances the migration of arterial smooth muscle cells through expression of the viral chemokine receptor US28 [37]. Conversely, HCMV impairs the migration of epithelial (cytotrophoblasts) [16] or endothelial [38] placenta cells through PPARγ activation or downregulation of angiogenesis genes, respectively.

We also observed strong immunostaining for LIS1 and DCX in histological sections of cases infected by HCMV compared with sections from control cases, which showed no or weak immunostaining (Figures 3 and 4). Key events in neuronal migration occur between the fifth and 22nd gestational weeks of human development [27]. The gestational age (23 weeks) of the four cases reported herein is consistent with the occurrence of pathogenic events occurring within this period of development. To our knowledge, histological analysis of LIS1 expression during development is not documented. In contrast, it has been shown that DCX expression is detectable only within the first 20 gestational weeks in the human fetal cerebrum [39]. This finding is consistent with our results, with the absence of DCX immunostaining in the brains of the control cases, also aged 23 gestational weeks. We have previously shown the immunohistochemical presence of the HCMV antigen IE in the same cases as the present study [11]. IE^+ cells are localised in a few discrete foci scattered throughout the brain parenchyma or in vessels. This pattern clearly does not overlap with that of LIS1 or DCX in the infected samples. It is, however, still possible that a non-cell autonomous effect, not detected in cultured NSCs, underlies increased LIS1 levels in the infected fetal brain. We had reported PPARγ activation in HCMV-infected fetal brains [11]. In that study, PPARγ and IE immunostainings did not overlap in histological samples. Yet we showed that infected NSCs were able to trigger PPARγ overexpression in uninfected neighbouring cells by releasing specific activating lipids. It is therefore likely that LIS1 overexpression might also be triggered by soluble mediators of unknown origin in the infected fetal brain. Such a bystander effect could possibly be of glial origin since it was not detected in NSC cultures. Because *PAFAH1B1* and *DCX* mutations are both causative in hereditary disorders of gyration including lissencephaly, we propose herein that their dysregulated expression at least contributes to gyration abnormalities in severe congenital HCMV infection. Mutational events leading to either haploinsufficiency or overexpression of *PAFAH1B1* are primary causes in a spectrum of neurodevelopmental disorders. Most documented are the cases when haploinsufficiency of *PAFAH1B1* causes classic lissencephaly (OMIM #607432) [40]. However, classic lissencephaly includes subcortical band heterotopia, which consists of circumferential bands of heterotopic neurons underneath the cortex. To our knowledge, this feature has never been reported upon HCMV congenital infection. Conversely, *PAFAH1B1* microduplications are associated with brain malformations, such as microcephaly or ventriculomegaly, and cognitive impairment [40,41]. *PAFAH1B1* duplications likely result in increased expression because gene dosage is consistent with copy number in autosomes [42,43]. Accordingly, increased expression of *PAFAH1B1* mRNA in lymphocytes from a patient with duplicated *PAFAH1B1* has been reported [41]. A transgenic mouse conditionally overexpressing LIS1 in the developing brain showed a decrease in brain size and a distorted cellular organisation in the ventricular zone [41]. Altogether, these findings underscore that LIS1 dosage must be finely tuned for proper brain development. A recent study revealed that mutations within *PAFAH1B1* or *DCX* accounted for the majority of lissencephaly cases [26]. Therefore, it is very likely that the unbalanced expression of *PAFAH1B1* and *DCX* in the HCMV-infected developing brain underlies brain dysgenesis. Abnormal neural cell migration was reported to be associated with cognitive impairment independently of the infectious context [6]. Thus, similar pathogenic events could possibly underlie mental retardation in mild cases of congenital HCMV infection.

It is likely that the timing and extent of infection, the nature of its molecular targets other than *PAFAH1B1*,

and the host immune response also modulate the nature and severity of sequelae.

Given the heterogeneity of the phenotypes due to duplications of *PAFAH1B1*, more work is needed to formally correlate LIS1 levels in the developing brain with the severity of the outcomes of HCMV infection. Indeed, LIS1 expression levels in the four cases presented here were not increased to the same extent, with no apparent relation with the severity of sequelae. An association study between *PAFAH1B1* variants and the severity of the outcomes of the infection in mildly or severely affected cases could allow the identification of possible severity markers. Indeed, HCMV alters gene expression by subverting the activity of a variety of host transcription factors [15,44]. We have carried out *in silico* analysis of conserved transcription factor binding sites (TFBSs) within *PAFAH1B1*. We identified that conserved putative responsive elements to PPARγ, AP1, and CREB were located within the 5' proximal promoter region of *PAFAH1B1*, or in its first intron (sequence details available upon request). Also, a frequent polymorphism within the 3' untranslated region of *PAFAH1B1* has been identified [45]. Since PPARγ, AP1, and CREB are triggered by HCMV infection [11,15,44], any hypothetical variation within these segments could possibly modify the response of *PAFAH1B1* to HCMV infection.

In conclusion, our findings reveal that *PAFAH1B1* is a critical target of congenital HCMV infection and a plausible contributor to the pathogenesis of brain sequelae. They also shine a new light on the pathophysiological bases of congenital HCMV infection by suggesting as well that defective neural cell migration may contribute to the neurodevelopmental sequelae of infection.

Acknowledgements

The present study was founded by institutional grants from INSERM, the CNRS and University of Toulouse. We wish to thank the AP-HP staff for collection of samples and F Capilla and C Salon from the US006 INSERM histology facility. We thank S Allart, A Canivet-Laffitte and D Daviaud for technical assistance at the cellular imaging facility TRI-CPTP, Toulouse. We also thank A Thouard for technical help and R Liblau, C Malnou, A Saoudi and E Suberbielle for their critical reading of the manuscript and useful comments. I-Stem is part of the Biotherapies Institute for Rare Diseases (BIRD).

Author contributions statement

MR carried out experiments and analysed data. MB, HM and YS carried out experiments. AB, BB, JA and ML-V provided samples or cells. DGD analysed data and wrote the manuscript. SC performed study design, carried out experiments, analysed data and wrote the manuscript. All the authors had final approval of the submitted and published versions.

References

1. Zuhair M, Smit GSA, Wallis G, *et al*. Estimation of the worldwide seroprevalence of cytomegalovirus: a systematic review and meta-analysis. *Rev Med Virol* 2019; **29:** e2034.
2. Cannon MJ. Congenital cytomegalovirus (CMV) epidemiology and awareness. *J Clin Virol* 2009; **46**(suppl 4): S6–S10.
3. Cheeran MC, Lokensgard JR, Schleiss MR. Neuropathogenesis of congenital cytomegalovirus infection: disease mechanisms and prospects for intervention. *Clin Microbiol Rev* 2009; **22:** 99–126.
4. White AL, Hedlund GL, Bale JF Jr. Congenital cytomegalovirus infection and brain clefting. *Pediatr Neurol* 2014; **50:** 218–223.
5. Stouffer MA, Golden JA, Francis F. Neuronal migration disorders: focus on the cytoskeleton and epilepsy. *Neurobiol Dis* 2016; **92:** 18–45.
6. Guerrini R, Parrini E. Neuronal migration disorders. *Neurobiol Dis* 2010; **38:** 154–166.
7. Fry AE, Cushion TD, Pilz DT. The genetics of lissencephaly. *Am J Med Genet C Semin Med Genet* 2014; **166:** 198–210.
8. Tsutsui Y, Kosugi I, Kawasaki H, *et al*. Roles of neural stem progenitor cells in cytomegalovirus infection of the brain in mouse models. *Pathol Int* 2008; **58:** 257–267.
9. Luo MH, Hannemann H, Kulkarni AS, *et al*. Human cytomegalovirus infection causes premature and abnormal differentiation of human neural progenitor cells. *J Virol* 2010; **84:** 3528–3541.
10. Belzile JP, Stark TJ, Yeo GW, *et al*. Human cytomegalovirus infection of human embryonic stem cell-derived primitive neural stem cells is restricted at several steps but leads to the persistence of viral DNA. *J Virol* 2014; **88:** 4021–4039.
11. Rolland M, Li X, Sellier Y, *et al*. PPARγ is activated during congenital cytomegalovirus infection and inhibits neuronogenesis from human neural stem cells. *PLoS Pathog* 2016; **12:** e1005547.
12. Han D, Byun SH, Kim J, *et al*. Human cytomegalovirus IE2 protein disturbs brain development by the dysregulation of neural stem cell maintenance and the polarization of migrating neurons. *J Virol* 2017; **91:** e00799-17.
13. Odeberg J, Wolmer N, Falci S, *et al*. Human cytomegalovirus inhibits neuronal differentiation and induces apoptosis in human neural precursor cells. *J Virol* 2006; **80:** 8929–8939.
14. Odeberg J, Wolmer N, Falci S, *et al*. Late human cytomegalovirus (HCMV) proteins inhibit differentiation of human neural precursor cells into astrocytes. *J Neurosci Res* 2007; **85:** 583–593.
15. Fortunato EA, McElroy AK, Sanchez I, *et al*. Exploitation of cellular signaling and regulatory pathways by human cytomegalovirus. *Trends Microbiol* 2000; **8:** 111–119.
16. Leghmar K, Cenac N, Rolland M, *et al*. Cytomegalovirus infection triggers the secretion of the PPAR gamma agonists 15-hydroxyeicosatetraenoic acid (15-HETE) and 13-hydroxyoctadecadienoic acid (13-HODE) in human cytotrophoblasts and placental cultures. *PLoS One* 2015; **10:** e0132627.
17. Schneider CA, Rasband WS, Eliceiri KW. NIH Image to ImageJ: 25 years of image analysis. *Nat Methods* 2012; **9:** 671–675.
18. Saillour Y, Carion N, Quelin C, *et al*. Lis1-related isolated lissencephaly: spectrum of mutations and relationships with malformation severity. *Arch Neurol* 2009; **66:** 1007–1015.
19. Vallee RB, Tsai J-W. The cellular roles of the lissencephaly gene LIS1, and what they tell us about brain development. *Genes Dev* 2006; **20:** 1384–1393.
20. Wynshaw-Boris A, Gambello MJ. LIS1 and dynein motor function in neuronal migration and development. *Genes Dev* 2001; **15:** 639–651.
21. Kato M, Dobyns WB. Lissencephaly and the molecular basis of neuronal migration. *Hum Mol Genet* 2003; **12:** R89–R96.
22. Spector DH. Human cytomegalovirus riding the cell cycle. *Med Microbiol Immunol* 2015; **204:** 409–419.
23. Castillo JP, Kowalik TF. Human cytomegalovirus immediate early proteins and cell growth control. *Gene* 2002; **290:** 19–34.

24. Landgren H, Curtis MA. Locating and labeling neural stem cells in the brain. *J Cell Physiol* 2011; **226:** 1–7.
25. Caspi M, Atlas R, Kantor A, *et al*. Interaction between LIS1 and doublecortin, two lissencephaly gene products. *Hum Mol Genet* 2000; **9:** 2205–2213.
26. Di Donato N, Timms AE, Aldinger KA, *et al*. Analysis of 17 genes detects mutations in 81% of 811 patients with lissencephaly. *Genet Med* 2018; **20:** 1354.
27. Wynshaw-Boris A. Lissencephaly and LIS1: insights into the molecular mechanisms of neuronal migration and development. *Clin Genet* 2007; **72:** 296–304.
28. Smith DS, Niethammer M, Ayala R, *et al*. Regulation of cytoplasmic dynein behaviour and microtubule organization by mammalian Lis1. *Nat Cell Biol* 2000; **2:** 767–775.
29. Sapir T, Elbaum M, Reiner O. Reduction of microtubule catastrophe events by LIS1, platelet-activating factor acetylhydrolase subunit. *EMBO J* 1997; **16:** 6977–6984.
30. Bechler ME, Doody AM, Racoosin E, *et al*. The phospholipase complex PAFAH Ib regulates the functional organization of the Golgi complex. *J Cell Biol* 2010; **190:** 45–53.
31. Bock HH, May P. Canonical and non-canonical reelin signaling. *Front Cell Neurosci* 2016; **10:** 166.
32. Tokuoka SM, Ishii S, Kawamura N, *et al*. Involvement of platelet-activating factor and LIS1 in neuronal migration. *Eur J Neurosci* 2003; **18:** 563–570.
33. Vallee RB, Faulkner NE, Tai CY. The role of cytoplasmic dynein in the human brain developmental disease lissencephaly. *Biochim Biophys Acta* 2000; **1496:** 89–98.
34. Buchsbaum IY, Cappello S. Neuronal migration in the CNS during development and disease: insights from *in vivo* and *in vitro* models. *Development* 2019; **146:** dev163766.
35. Reiner O. LIS1 and DCX: implications for brain development and human disease in relation to microtubules. *Scientifica (Cairo)* 2013; **2013:** 393975.
36. Collins-McMillen D, Stevenson EV, Kim JH, *et al*. Human cytomegalovirus utilizes a nontraditional signal transducer and activator of transcription 1 activation cascade via signaling through epidermal growth factor receptor and integrins to efficiently promote the motility, differentiation, and polarization of infected monocytes. *J Virol* 2017; **91:** e00622–e00617.
37. Streblow DN, Soderberg-Naucler C, Vieira J, *et al*. The human cytomegalovirus chemokine receptor US28 mediates vascular smooth muscle cell migration. *Cell* 1999; **99:** 511–520.
38. Gustafsson RKL, Jeffery HC, Yaiw K-C, *et al*. Direct infection of primary endothelial cells with human cytomegalovirus prevents angiogenesis and migration. *J Gen Virol* 2015; **96:** 3598–3612.
39. Mizuguchi M, Qin J, Yamada M, *et al*. High expression of doublecortin and KIAA0369 protein in fetal brain suggests their specific role in neuronal migration. *Am J Pathol* 1999; **155:** 1713–1721.
40. Blazejewski SM, Bennison SA, Smith TH, *et al*. Neurodevelopmental genetic diseases associated with microdeletions and microduplications of chromosome 17p13.3. *Front Genet* 2018; **9:** 80.
41. Bi W, Sapir T, Shchelochkov OA, *et al*. Increased LIS1 expression affects human and mouse brain development. *Nat Genet* 2009; **41:** 168–177.
42. Tang YC, Amon A. Gene copy-number alterations: a cost–benefit analysis. *Cell* 2013; **152:** 394–405.
43. Pires JC, Conant GC. Robust yet fragile: expression noise, protein misfolding, and gene dosage in the evolution of genomes. *Annu Rev Genet* 2016; **50:** 113–131.
44. Paulus C, Nevels M. The human cytomegalovirus major immediate-early proteins as antagonists of intrinsic and innate antiviral host responses. *Viruses* 2009; **1:** 760–779.
45. Koch A, Tonn J, Albrecht S, *et al*. Frequent intragenic polymorphism in the 3' untranslated region of the lissencephaly gene 1 (LIS-1). *Clin Genet* 2008; **50:** 527–528.

SUPPLEMENTARY MATERIAL ONLINE

Supplementary figure legends

Figure S1. Immunofluorescence analysis of HCMV-infected (HCMV) or uninfected (NI) NSCs with antibodies to IE (green) or alpha-tubulin (red)

Figure S2. Immunofluorescence analysis of HCMV-infected (HCMV) or uninfected (NI) MRC-5 cells, using antibodies to IE (green) or LIS1 (red)

Figure S3. Ki-67 analysis of NSCs

Figure S4. Immunofluorescence analyses of HCMV-infected (HCMV) or uninfected (NI) NSCs or HIPEC cells, treated with either LIS1-siRNA (siLIS1) or non-targeting siRNA (siNT)

Figure S5. Immunofluorescence analysis of HCMV-infected (HCMV) or uninfected (NI) NSCs, using antibodies to IE (green) or DCX (red)

Table S1. RT^2 profiler analysis of neuronogenesis-related genes in HCMV-infected NSCs

Table S2. RT^2 profiler analysis of neuronogenesis-related genes in HCMV-infected MRC-5 cells

Movies S1–S4. 3D reconstructions of immunofluorescence analyses of HCMV-infected NSCs